J. Fluid Mech. (1978), *vol.* 87, *part* 1, *pp.* 159–178
Printed in Great Britain

The unsteady motion of a two-dimensional aerofoil in incompressible inviscid flow

By B. C. BASU AND G. J. HANCOCK

Department of Aeronautical Engineering, Queen Mary College,
Mile End Road, London E1 4NS

(Received 24 January 1977 and in revised form 29 September 1977)

A numerical method has been developed for the calculation of the pressure distribution, forces and moments on a two-dimensional aerofoil undergoing an arbitrary unsteady motion in an inviscid incompressible flow. In a discussion of the appropriate Kutta condition(s) it is argued that two Kutta conditions are required to obtain a satisfactory solution. The method is applied to (i) a sudden change in aerofoil incidence, (ii) an aerofoil oscillating at high frequency and (iii) an aerofoil passing through a sharp-edged gust.

1. On the Kutta condition

In this paper a numerical method is formulated to solve the flow about a two-dimensional aerofoil which is performing some kind of time-dependent motion in an incompressible inviscid fluid. As in all problems concerning aerofoils in inviscid flow, auxiliary conditions need to be invoked to ensure that a unique solution is obtained. These conditions, known as the Kutta conditions, relate to assumptions about the flow characteristics at, or at least in the neighbourhood of, the aerofoil trailing edge. To some extent this paper is concerned with the elucidation of the appropriate Kutta condition(s) to give a consistent mathematical model as a basis for a numerical solution. Before presenting the formulation of the unsteady mathematical model, some general comments on the Kutta conditions are made.

Consider first an aerofoil at a steady small angle of incidence in a steady inviscid incompressible stream. It is implicit in the statement of this problem that the aim is to represent the characteristics of the steady aerofoil in a real, viscous fluid flow at high Reynolds number. When the flow is attached the effects of viscosity are confined to thin boundary layers on the aerofoil surface and to the downstream wake formed by the merging of the upper and lower surface boundary layers at the aerofoil trailing edge. As a first approximation it is reasonable to assume that the flow can be regarded as inviscid so long as the flow in the region of the trailing edge remains 'sensible'; that is, no infinities in either flow velocities or in the pressure should appear in the solution at the sharp trailing edge. It is common practice to regard the inviscid solution as a first stage in an iterative procedure for the real flow solution; in subsequent stages the displacement effects of the boundary layer and wake are superimposed on the aerofoil surface and the inviscid solution around a displaced surface, no longer closed, is determined.

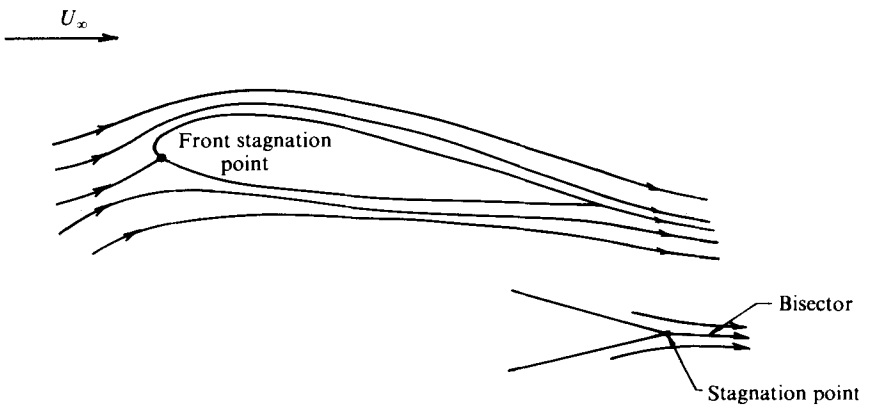

FIGURE 1. Steady aerofoil in inviscid flow: analytic solution.

Analytic solutions for steady lifting aerofoils of special profile in a steady incompressible inviscid stream can be obtained from conformal transformation techniques (Glauert 1947), in which the inviscid flow about the aerofoil is transformed into the inviscid flow about a circular cylinder. The standard unique solution is obtained using the Kutta condition that velocities remain finite at the trailing edge; the trailing-edge point for a non-zero trailing-edge angle is then a stagnation point and the dividing streamline from the trailing edge bisects the tangents from the upper and lower surfaces at the trailing edge as shown in figure 1. In this analytic solution, although the velocities, and pressures, remain finite at the trailing edge, the flow at the trailing edge itself is singular in the sense that the rates of change of the surface velocities are infinite there. It should also be noted that all solutions for the inviscid flow past a steady aerofoil when the separation point lies on either the upper or the lower surface (i.e. when the flow does not separate at the trailing edge) necessarily have infinite velocities and pressures at the trailing edge, and the loading (i.e. the difference between the pressures on the upper and lower surfaces) is also infinite at the trailing edge for a non-zero trailing-edge angle.

For those steady aerofoils in a uniform stream not amenable to solution by conformal transformation, a direct numerical method can be applied; the most popular technique is associated with Hess & Smith (1967). One variant of this method (Hancock & Padfield 1972) is shown in figure 2; the aerofoil surface is divided into N straight-line elements, starting with element 1 on the lower surface at the trailing edge and proceeding clockwise around the aerofoil contour; so that element N is on the upper surface at the trailing edge. A uniform source distribution σ_i and a uniform vorticity distribution γ are placed on the ith element; the source strength σ_i varies from element to element but the vorticity strength γ is the same for all elements. The boundary condition of tangential flow over the aerofoil surface is satisfied by taking the resultant velocity at the exterior midpoint of each element to be tangential to that element; thus

$$(q_n)_j = 0, \tag{1}$$

where $(q_n)_j$ is the total normal velocity at the external midpoint of the jth element due to the free stream and the velocities induced by the source and vorticity distributions. For the Kutta condition, the tangential velocities $(q_t)_1$ and $(q_t)_N$ in the downstream

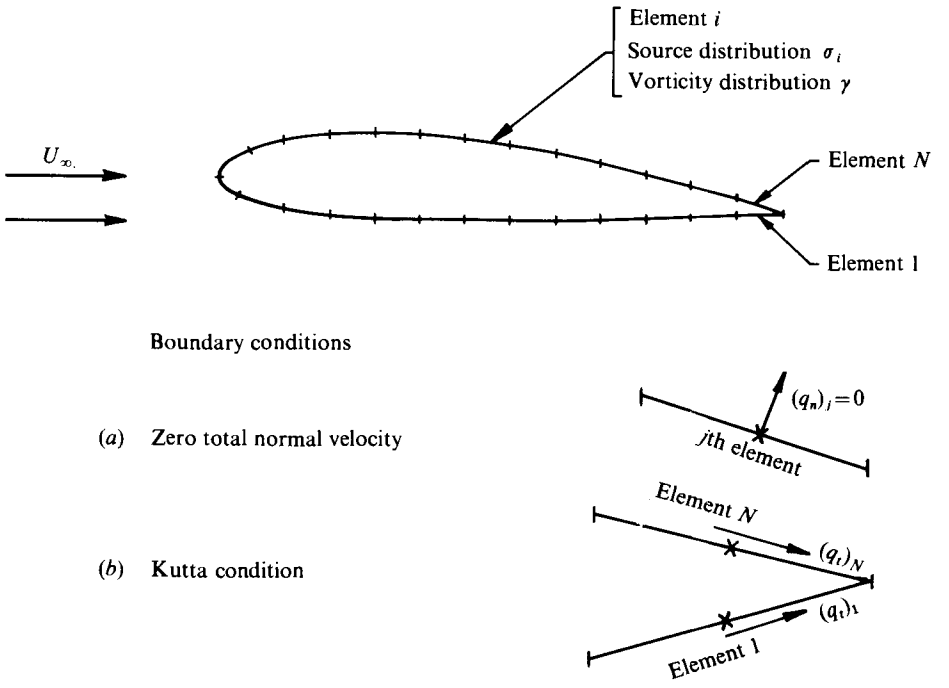

FIGURE 2. Model for the steady inviscid numerical solution.

direction at the midpoints of the two elements at the trailing edge are made equal. These conditions give $N+1$ linear simultaneous equations from which the $N+1$ unknowns σ_i $(i = 1, \ldots, N)$ and γ can be calculated. In this numerical solution the basis of the Kutta condition is that if the (tangential) surface velocities in the downstream direction in the neighbourhood of the trailing edge are equal in magnitude then no vorticity can be shed aft of the aerofoil; this is consistent with the circulation around the wing remaining constant. When the surface velocities are made equal at the midpoints of the trailing-edge elements then, by the Bernoulli equation, the pressures at these points are also equal, so the Kutta condition can be reinterpreted as the condition of zero loading in the region of the trailing edge, which is physically realistic.

In the above numerical solution the actual trailing edge is not a stagnation point; in fact the velocities there are infinite as they are at the ends of all elements. Furthermore it is found that the velocities at the midpoints of the trailing-edge elements differ significantly from stagnation values; they are more likely to be closer to the free-stream velocity. In the numerical solution the flow characteristics are essentially averaged over the length of an element, thus the exact analytic singular behaviour in the neighbourhood of the rear stagnation point at the trailing edge is averaged over the trailing-edge elements. Analytical and numerical results for most aerofoils are virtually identical except in the region very close to the trailing edge, as shown in figure 3, in spite of the alternative forms of the Kutta condition.

It is argued that there is no definitive statement of *the* Kutta condition for a steady aerofoil, each mathematical model requiring its own consistent 'Kutta' condition to ensure a unique solution; the relevant and appropriate Kutta condition needs to be formulated separately for each mathematical model.

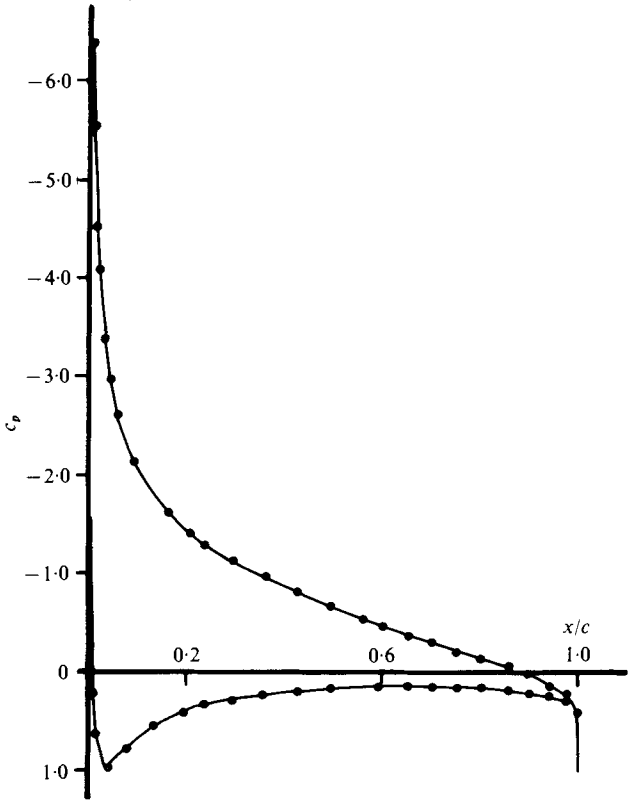

FIGURE 3. Comparison of analytic solution (curve) and numerical solution (points) for a 13% thick symmetrical Kármán–Trefftz aerofoil. $\alpha = 10°$, c = chord.

Attention is now turned to the case where the aerofoil is moving relative to a steady incompressible inviscid stream. As indicated in figure 4(*a*), the circulation $\Gamma(t)$ around the aerofoil varies with time t. Since the total circulation around the aerofoil and wake must be zero, circulation of strength $(\partial\Gamma/\partial t)\,\delta t$ is shed aft of the aerofoil in a time δt and this shed vorticity is then convected downstream. The behaviour of the flow in the region of the trailing edge is now considered.

Suppose that the flow separates from the trailing edge, as shown in figure 4(*b*), where it is implied that the trailing edge is a conventional stagnation point. Then the flow approaching the trailing edge T on both the upper surface UT and the lower surface LT will tend to zero. Although the velocities on the upper and lower surfaces become equal on approaching T, the pressures do not tend to the same values because in the application of the unsteady Bernoulli equation a discontinuity in $\partial\phi/\partial t$ exists which is associated with $\partial\Gamma/\partial t$. A finite pressure difference at the trailing edge is unacceptable on physical grounds. The solution sought should have no infinities in either the velocity or the pressure at the trailing edge.

To meet these conditions Maskell (1972) argues that the flow must leave the trailing edge parallel either to the upper surface or to the lower surface depending on the sign of the shed vorticity. When the shed vorticity is anticlockwise the flow leaves the trailing edge parallel to the lower surface as shown in figure 4(*c*), whereas when the

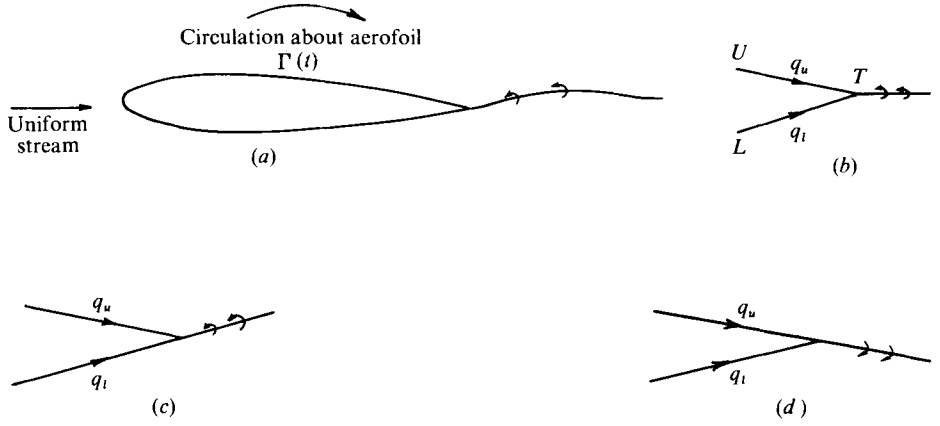

FIGURE 4. (*a*) Aerofoil moving relative to a steady inviscid stream. (*b*) 'Separation' at trailing edge. (*c*), (*d*) 'Maskell' trailing-edge flows.

shed vorticity is clockwise the flow leaves the trailing edge parallel to the upper surface as shown in figure 4 (*d*). For the flow shown in figure 4 (*c*), the velocity q_u on the upper surface tends to zero at the trailing edge while the velocity q_l on the lower surface remains finite; the pressure difference is zero upstream of the trailing edge provided that

$$0 = p_l - p_u = -\rho\,\partial\phi_l/\partial t + \rho\,\partial\phi_u/\partial t - \tfrac{1}{2}\rho q_l^2 + \tfrac{1}{2}\rho q_u^2, \tag{2}$$

i.e.

$$\partial(\phi_l - \phi_u)/\partial t = \partial\Gamma/\partial t = \tfrac{1}{2}q_l^2. \tag{3}$$

Equation (3) is compatible with convection of shed vorticity at the trailing edge with the local velocity since aft of the trailing edge

$$(\partial\Gamma/\partial t)\,\delta t = q_l \delta s;$$

thus

$$\partial\Gamma/\partial t = q_l(\delta s/\delta t)_{\delta t \to 0} = \tfrac{1}{2}q_l^2 \tag{4}$$

since $(\delta s/\delta t)_{\delta t \to 0}$ is equal to $\frac{1}{2}q_l$, the mean of the two velocities either side of the shed vortex sheet. Giesing (1969) came to the same conclusion by following a slightly different approach.

A consequence of the above argument is the recognition that the steady state is not a simple limit of an unsteady problem as $\partial\Gamma/\partial t$ tends to zero. According to the above argument the flow always leaves the trailing edge parallel to either the upper or the lower surface whatever the magnitude of $\partial\Gamma/\partial t$ as long as $\partial\Gamma/\partial t \neq 0$. However, when $\partial\Gamma/\partial t$ is identically zero the flow leaves the trailing edge along the bisector of the trailing-edge angle. It is postulated, although no proof has yet been given, that in the unsteady problem the curvature of the streamline emanating from the trailing edge in the region of the trailing edge tends to infinity as $\partial\Gamma/\partial t \to 0$. In this manner the unsteady problem degenerates into the known steady solution.

Maskell's solution in the region of the trailing edge arises from the assumptions that the loading across the shed vorticity in the wake is zero and that the velocities at the trailing edge remain finite; thus separation takes place from the sharp trailing edge and the loading across the trailing edge is zero for consistency with the condition of zero loading across the shed vorticity.

Up to the present time, as far as the authors are aware, there is no analytic solution for an aerofoil undergoing an unsteady motion which satisfies both the condition of finite velocities and the condition of zero loading at the trailing edge. The most elegant analytic solution is due to van der Vooren & van der Vel (1964) and is based on a conformal mapping of a particular aerofoil oscillating in pitch or in heave into a stationary circle. Their Kutta condition makes the point on the circle corresponding to the trailing edge in the physical plane a stagnation point. This Kutta condition gives zero loading and smooth flow at the trailing edge only when the trailing edge is a cusp. For non-zero trailing-edge angles two singularities appear in the expression for the pressure; the removal of the larger velocity singularity leaves a weaker singularity which prevents smooth outflow and which implies a pressure discontinuity both at the trailing edge and downstream across the wake.

The most comprehensive numerical solution is due to Giesing (1969) and is based on the Hess & Smith procedure. The Kutta condition invoked here is velocities equal in both magnitude and (downstream) direction at the midpoint of the two trailing-edge elements. The implication is that there is not only a finite loading across the trailing edge but also a finite loading across the shed vorticity in the wake just downstream of the trailing edge.

For general unsteady motions it is possible to obtain numerical solutions by imposing either the condition of finite velocities about the trailing edge or the condition of zero loading about the trailing edge. It is argued that the appropriate solution should satisfy both conditions in the neighbourhood of the trailing edge.

Here the basic numerical approach of Giesing (1968) is used but the conditions in the region of the trailing edge are modified. Since this approach is a numerical one the Kutta condition(s) have to be formulated for consistency with the mathematical model, and it is not admissible to use the local analytic Maskell trailing-edge flow with its singular behaviour involving infinite rates of change of velocity, etc. In the numerical solution described here it is ensured that the flow separates from the trailing edge, that there is zero loading across the vorticity shed from the trailing edge just downstream of the trailing edge, and that there is zero loading across the two trailing-edge elements on the aerofoil surface either side of the trailing edge. No direct attempt is made to limit the trailing-edge velocities but these velocities necessarily remain finite because of the above conditions.

In §2 the numerical model is formulated and the numerical procedure is outlined. In §§ 3, 4 and 5 the results are discussed for an aerofoil undergoing a sudden change in incidence, an aerofoil oscillating in pitch at high frequency and an aerofoil passing through a sharp-edged gust.

2. Numerical solution for the unsteady motion of an aerofoil

The solution for the flow about an aerofoil undergoing an arbitrary time-dependent motion which started at $t = 0$ is calculated at successive intervals of time

$$t_k \quad (t_0 = 0, \quad k = 1, 2, 3, \ldots)$$

by a method based on the Hess & Smith approach. At time t_k the model is as shown in figure 5.

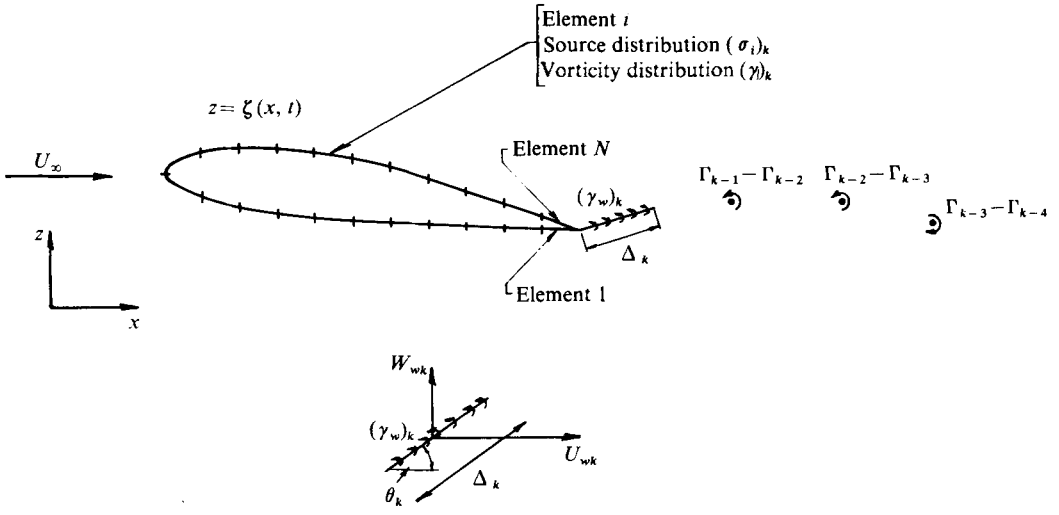

FIGURE 5. Solution at time t_k.

The aerofoil contour at time t_k is replaced by N straight-line elements. A uniform source distribution $(\sigma_i)_k$ and a uniform vorticity distribution γ_k are placed on the ith element ($i = 1, \ldots, N$), where $(\sigma_i)_k$ varies from element to element, γ_k is the same for all elements on the aerofoil and the subscript k refers to the time t_k. The overall circulation Γ_k is $\gamma_k \times$ (aerofoil perimeter). A small straight-line wake element of length Δ_k and inclined at an angle θ_k to the Ox axis (i.e. the free-stream direction) is attached to the trailing edge. The length Δ_k and the inclination θ_k are arbitrary at this stage; their values are to be determined as part of the solution. The vorticity on the trailing-edge wake element is $(\gamma_w)_k$, where

$$\Delta_k(\gamma_w)_k = \Gamma_k - \Gamma_{k-1}. \tag{5}$$

Thus the circulation on the element is the change in circulation around the aerofoil between times t_{k-1} and t_k, assuming that Γ_{k-1} has already been evaluated. A downstream wake of concentrated vortices is formed from the vorticity shed at earlier times, which is assumed to be concentrated into discrete vortices and convected according to the resultant velocities calculated at the centre of each vortex at each successive time interval. Thus the pattern of the downstream discrete vortices, their strengths and their positions are regarded as known at time t_k.

Thus at time t_k there are $N+3$ unknowns $(\sigma_i)_k$ ($i = 1, \ldots, N$), γ_k, Δ_k and θ_k. The basic set of equations can be formulated as follows.

(i) The N conditions of zero normal flow at the external midpoint of each aerofoil element are

$$(Q_{nj})_k = 0, \tag{6}$$

where $(Q_{nj})_k$ is the total normal velocity at the exterior midpoint of the jth element at time t_k.

(ii) The condition of equal pressures at the midpoint of the two elements on the aerofoil on either side of the trailing edge is

$$(Q_{t1})_k^2 = (Q_{tN})_k^2 + 2(\Gamma_k - \Gamma_{k-1})/(t_k - t_{k-1}), \tag{7}$$

where $(Q_{t1})_k$ is the total tangential velocity at the midpoint of element 1 and $(Q_{tN})_k$ is the total tangential velocity at the midpoint of element N at time t_k.

(iii) The length and orientation of the trailing-edge wake element (i.e. Δ_k and θ_k) are determined from the condition that the element is tangential to the local resultant velocity and that its length is proportional to the local resultant velocity. If $(U_w)_k$ and $(W_w)_k$ are the total component velocities induced at the midpoint of the trailing-edge wake element, excluding the effect of the element on itself, then

$$\left.\begin{aligned} \tan\theta_k &= (W_w)_k/(U_w)_k \\ \text{and} \qquad \Delta_k &= [(U_w)_k^2+(W_w)_k^2]^{\frac{1}{2}}[t_k-t_{k-1}]. \end{aligned}\right\} \tag{8}$$

Since the problem is concerned with incompressible flow the formulae for the induction of velocities by source and vorticity distributions are the same as for the steady case; thus the experience gained with the steady Hess & Smith method carries over to the unsteady problem.

If $(\sigma_i)_k$ and γ_k are normalized with respect to c and U_∞, the normalized perturbation velocities at the midpoint of the outer surface of the jth element due to the distributions of sources and vorticity on the aerofoil can be expressed in the form

$$\left.\begin{aligned} (u_j)_k &= \sum_{i=1}^{N} A_{ji}(\sigma_i)_k+\gamma_k \sum_{i=1}^{N} B_{ji}, \\ (w_j)_k &= \sum_{i=1}^{N} B_{ji}(\sigma_i)_k-\gamma_k \sum_{i=1}^{N} A_{ji}, \end{aligned}\right\} \tag{9}$$

where A_{ji} and B_{ji} are the appropriate influence coefficients, which depend on the instantaneous co-ordinates of the ith and jth elements.

The normalized perturbation velocity components induced at the midpoint of the jth element by the small line wake element attached to the trailing edge can be expressed in the form

$$(u_{wj})_k = (\gamma_w)_k B_{jN+1}, \quad (w_{wj})_k = -(\gamma_w)_k A_{jN+1}. \tag{10}$$

The normalized perturbation velocity components induced at the midpoint of the jth element by the concentrated wake vortices $\bar{\Gamma}_m$ $(= \Gamma_m/U_\infty c)$ formed at earlier times can be expressed in the form

$$(u_{\Gamma j})_k = \sum_{m=1}^{k-1} C_{jm}\bar{\Gamma}_m, \quad (w_{\Gamma j})_k = \sum_{m=1}^{k-1} D_{jm}\bar{\Gamma}_m, \tag{11}$$

where C_{jm} and D_{jm} are the appropriate influence coefficients.

The total normalized perturbation velocity components are the sums of the components given in (9)–(11). These total normalized perturbation velocity components are superimposed on the mainstream components and substituted into the basic equations (6)–(8). The basic set of equations is nonlinear thus the following iterative procedure is adopted for its solution.

The values of Δ_k and θ_k are guessed, leaving N linear equations from (6) and a quadratic equation from (7). The N linear equations are solved to give

$$(\sigma_i)_k \quad (i = 1, \ldots, N)$$

in terms of γ_k, then γ_k is obtained from the quadratic equation obtained from (7). Once $(\sigma_i)_k$ $(i = 1, \ldots, N)$ and γ_k are known $(U_w)_k$ and $(W_w)_k$ can be calculated and substituted in (8) to find the new values of Δ_k and θ_k. The procedure is repeated until Δ_k and θ_k have converged to the desired accuracy.

Once the source and vorticity strengths have been determined the velocity distribution on the aerofoil is known from (9)–(11). The pressure coefficient follows from the unsteady Bernoulli equation, namely

$$c_p = 1 - \frac{Q^2}{U_\infty^2} - \frac{2}{U_\infty^2}\frac{\partial \phi}{\partial t}, \tag{12}$$

where Q is the total velocity on the outer aerofoil surface and ϕ is the velocity potential. The force and moment coefficients are obtained by direct integration of the pressure distributions.

In the calculation of the unsteady pressure coefficient, $\partial\phi/\partial t$ has to be determined. In the present numerical method the value of $\partial\phi/\partial t$ at the midpoint of the jth element at time t_k is approximated by

$$(\partial\phi/\partial t_j)_k = \{(\phi_j)_k - (\phi_j)_{k-1}\}/(t_k - t_{k-1}). \tag{13}$$

The velocity potential ϕ is obtained by integrating the velocity field along the x axis from upstream of the aerofoil and then around the aerofoil surface.

Once the solution at time t_k has been determined, the model is set up for time t_{k+1}, with the wake pattern as calculated from the solution at time t_k. The distributed vorticity on the wake element at time t_k is now assumed to be concentrated into a vortex of strength $(\gamma_w)_k \Delta_k$ at time t_{k+1} situated at

$$\left.\begin{aligned} x &= (x_{\text{trailing edge}})_k + \tfrac{1}{2}\Delta_k \cos\theta_k + (U_w)_k (t_{k+1} - t_k), \\ z &= (z_{\text{trailing edge}})_k + \tfrac{1}{2}\Delta_k \sin\theta_k + (W_w)_k (t_{k+1} - t_k). \end{aligned}\right\} \tag{14}$$

The resultant velocity at the centre of each of the other concentrated vortices in the wake is calculated from the solution at time t_k, then the position of that vortex at time t_{k+1} follows directly.

Programs have been developed in FORTRAN IV which can handle 35 elements on the aerofoil for a core size of 20 K, including the system and program.

The present numerical method has been applied to

(i) the time-dependent build-up of lift on an aerofoil which undergoes a sudden change in incidence from 0 to α at time $t = 0$,

(ii) an aerofoil which starts to oscillate about zero incidence at a high frequency,

(iii) an aerofoil passing through a sharp-edged gust.

3. Sudden change in incidence

The particular case considered for the calculation of the time-dependent build-up of lift is an 8·4 % thick symmetric Von Mises aerofoil with an incidence change from 0 to 0·1 rad at $t = 0$. The problem has been solved with short time intervals $\Delta t U_\infty/c$ of 0·005 for $0 < tU_\infty/c < 0{\cdot}3$, longer time intervals of 0·05 for intermediate times 0·3–0·5 and somewhat longer time intervals of 0·1 for times 0·5–2·0; thus it is hoped that the correct behaviour of the solution at small times, when the rates of change are rapid, has been obtained.

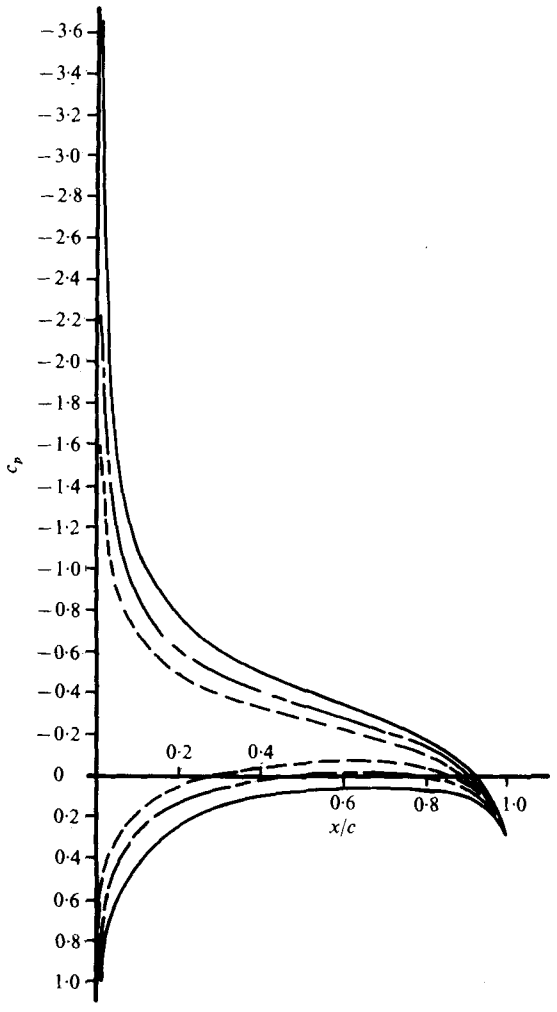

FIGURE 6. Pressure distribution on 8·4 % symmetrical Von Mises aerofoil after a sudden change in incidence. ——, $tU_\infty/c = \infty$; — — —, $tU_\infty/c = 2{\cdot}0$; – – –, $tU_\infty/c = 0{\cdot}2$.

The development of the pressure distribution with time is shown in figure 6. The starting vortex and its convection downstream after a time interval $tU_\infty/c = 2{\cdot}0$ are shown in figure 7(*a*). The build-up of the lift C_L/C_{LS}, where C_{LS} is the ultimate steady lift, is shown in figure 7(*b*). Although the curve appears to build up from zero with time it must be remembered that in this problem there is an impulsive lift at $t = 0$, which arises from the instantaneous change in ϕ; no attempt has been made to determine the impulsive loading at $t = 0$. The solution has been obtained at time $t_1(tU_\infty/c = 0{\cdot}005)$ and again at time $t_2(tU_\infty/c = 0{\cdot}01)$; the graph shown in figure 7(*b*) starts at t_2. For comparison the standard linearized solution (i.e. the Wagner function) is shown; also shown is the solution by Giesing (1968), in which the condition of flow separation at the trailing edge was satisfied but not the condition of zero loading. It is seen that there are significant differences among the various solutions up to $tU_\infty/c = 2{\cdot}0$.

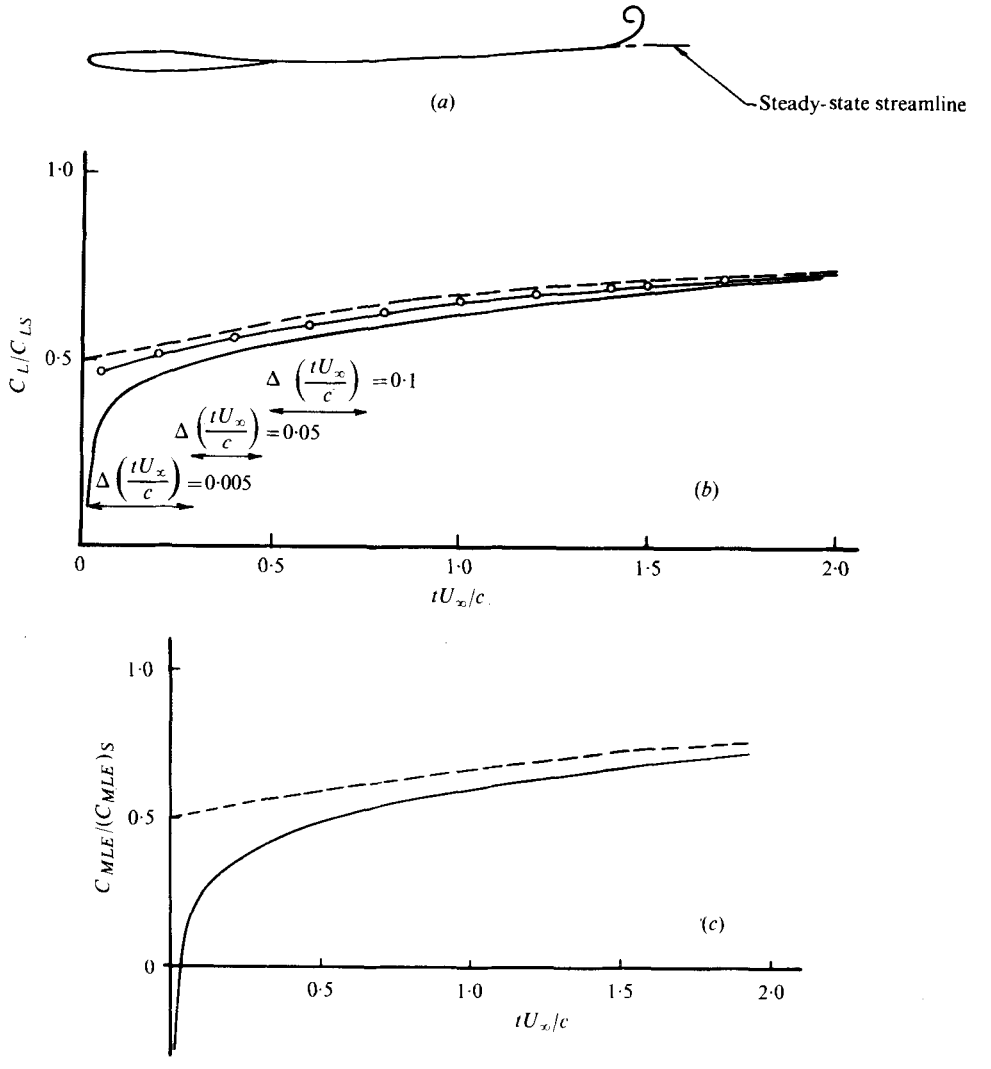

FIGURES 7(*a*)–(*c*). For legend see p. 170.

The moment coefficient about the leading edge is shown in figure 7(*c*). It is seen that at very small times there is a large nose-up pitching moment but then the moment changes sign; the centre of pressure approaches its final steady position near the quarter-chord point.

The variation of the drag coefficient with time is shown in figure 7(*d*). It is seen that with the build-up of lift the drag initially increases (up to about $tU_\infty/c = 1{\cdot}6$) then starts to reduce, becoming zero as $t \to \infty$. This result suggests that initially the build-up in the leading-edge suction lags behind the normal pressure to give a resultant drag force. This trend is confirmed by the pressure distribution at different times (figure 6).

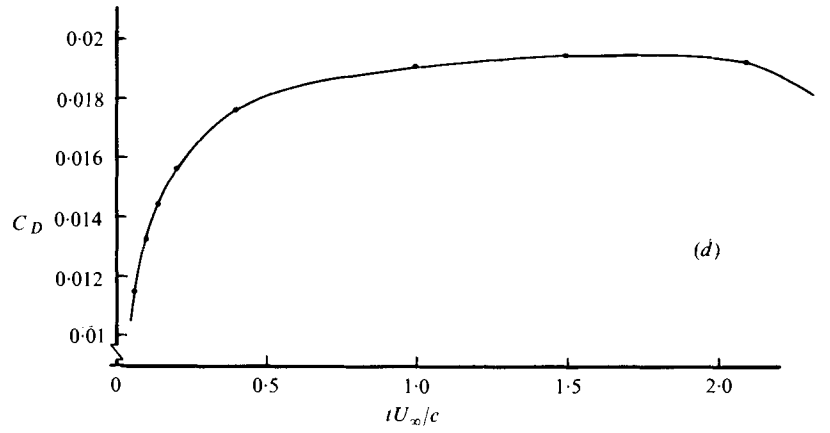

FIGURE 7. 8·4% symmetrical Von Mises aerofoil. (*a*) Wake vortex sheet at $tU_\infty/c = 2{\cdot}0$. (*b*) Growth of lift following sudden change in incidence (α increased from 0 to 0·1 rad). (*c*) Pitching moment about leading edge following sudden change in incidence. (*d*) Drag coefficient following sudden change in incidence. ---, linearized theory; —⊙—, Giesing; ——, present approach.

FIGURE 8. Vortex position at $tU_\infty/c = 1{\cdot}85$. 8·4% symmetrical Von Mises aerofoil in pitching oscillation; $\nu = 20$, $\theta_0 = 0{\cdot}573°$.

4. Aerofoil oscillations at a high frequency

The same aerofoil (i.e. an 8·4% thick symmetrical Von Mises aerofoil) is considered to be oscillating in pitch at a high frequency ($\nu = \omega c/U_\infty = 20$) with an amplitude of 0·01 rad (0·573°). The flow characteristics have been calculated at time intervals of 0·03927 up to $tU_\infty/c = 1{\cdot}84569$.

The wake pattern in figure 8 shows the rolling-up of the wake vorticity into vortices of opposite sign; the pattern closely follows observed patterns in real fluids. The behaviour of the wake in the trailing-edge region is shown in figure 9 for a half-cycle when periodic flow has become established. Starting when θ (the angle of pitch) is zero with θ increasing, the strengths of the shed vorticity are indicated and the conservation of the convected vorticity is seen at successive time intervals. As θ increases, anticlockwise vorticity is shed as expected; after θ reaches its maximum amplitude and begins to decrease, vorticity of opposite sign is shed; there is a phase lead in the direction of the shed vorticity as can be seen at $\theta = 0{\cdot}573°$, when the direction of the shed vorticity has already changed sign. It is seen that when θ returns to zero after a half-cycle the wake pattern is similar to the original pattern when θ was initially zero; the magnitude of the trailing vorticity is of the same magnitude but of opposite sign.

One of the most encouraging features of the numerical solution is the fact that the trailing-edge wake element is virtually parallel to either the upper or the lower aerofoil surface (e.g. at $\theta = 0, 0{\cdot}406°, 0{\cdot}406°, 0$) except when the sign of the vorticity is changing (at $\theta = 0{\cdot}573°$). So although the Kutta condition has not been specifically formulated

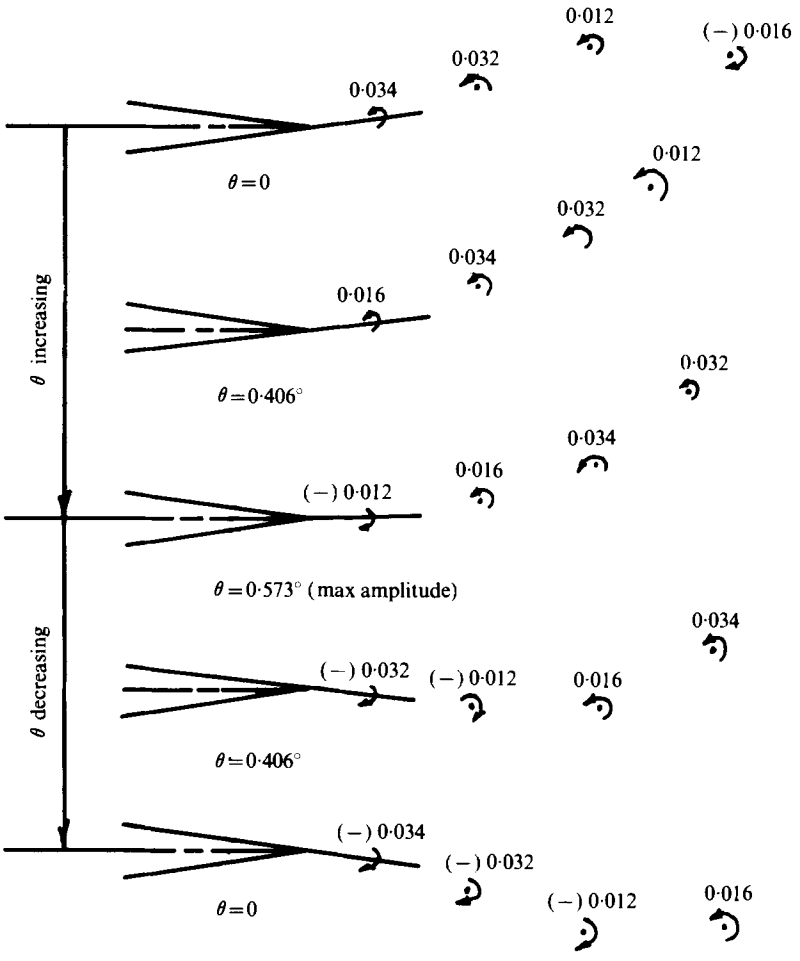

FIGURE 9. 8·4 % thick symmetrical Von Mises aerofoil oscillating about leading edge: theoretical characteristics in region of trailing edge.

in terms of tangential flow separation as postulated by Maskell, the present numerical solution seems to satisfy this tangential flow condition for most of the cycle.

Figure 10 shows the variation of C_L and C_M (about the leading edge) over one cycle five cycles after the start. Comparison is made with results obtained from a theory which is linearized in the amplitude of oscillation but uses the exact aerofoil profile (Basu & Hancock 1978). Also, results from the standard linearized theory are indicated. The results of the present numerical approach show that the variations in C_L and C_M are not quite simple harmonic owing to the skewness in the neighbourhood of the peak.

5. Aerofoil entering a sharp-edged gust

An aerofoil entering a sharp-edged vertical gust of velocity w_g is shown in figure 11. The gust boundary, which is a surface of discontinuity of vertical velocity, remains planar as long as the gust front is not too close to the aerofoil. As the gust front approaches the aerofoil and travels past it, the part of the gust front near the aerofoil

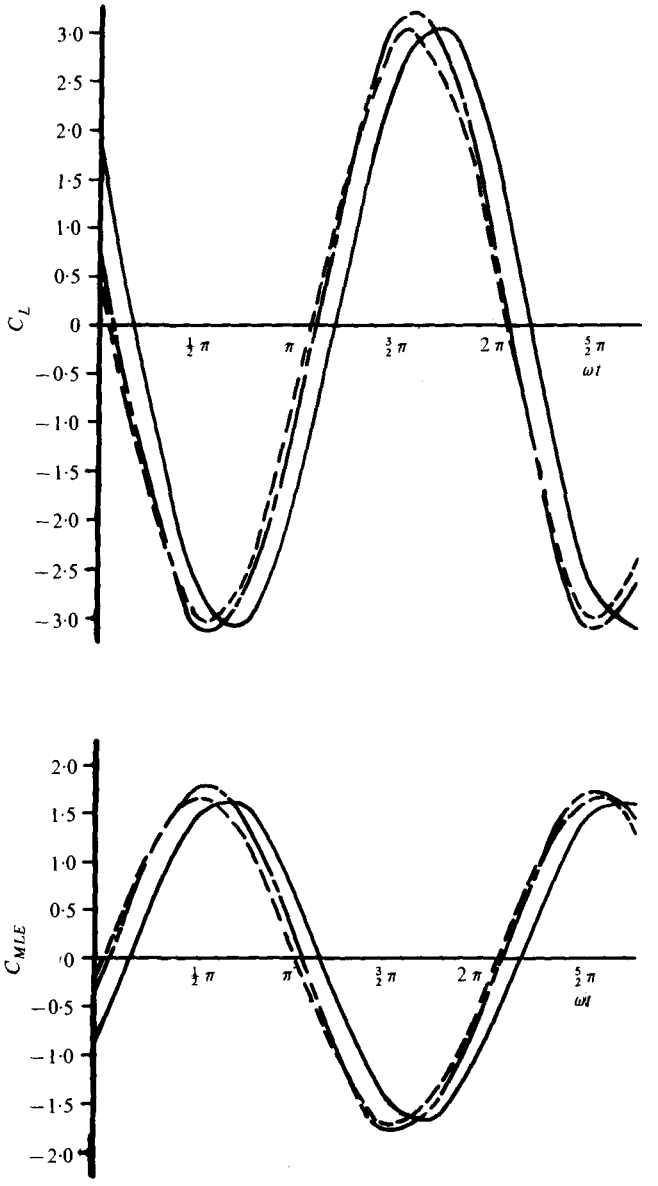

FIGURE 10. 8·4% symmetrical Von Mises aerofoil oscillating about leading edge; $\nu = 20$, $\theta_0 = 0{\cdot}573°$. – – –, linearized theory; ——, present approach; — — —, Basu & Hancock (1978).

surface is deformed under the influence of the aerofoil profile and the wake. For the calculation of the growth of the lift as the aerofoil passes through the vertical gust, it has been the usual practice to assume that the gust front remains undeformed as gust travels past the aerofoil and its wake. Such an assumption simplifies the numerical problem considerably, but for a more extensive treatment the deformation of the gust front should be taken into account. Here this is done by representing the gust front by a vortex sheet under the influence of the aerofoil and its wake. The present

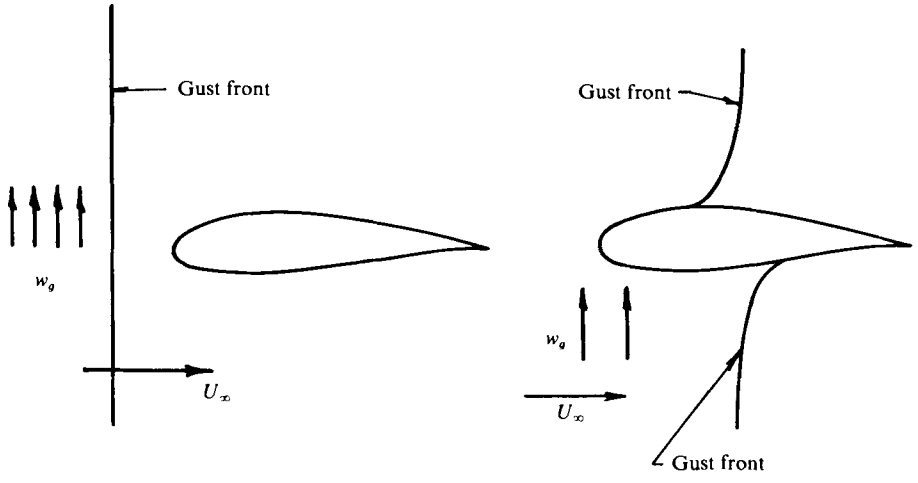

FIGURE 11. Aerofoil entering a vertical gust field.

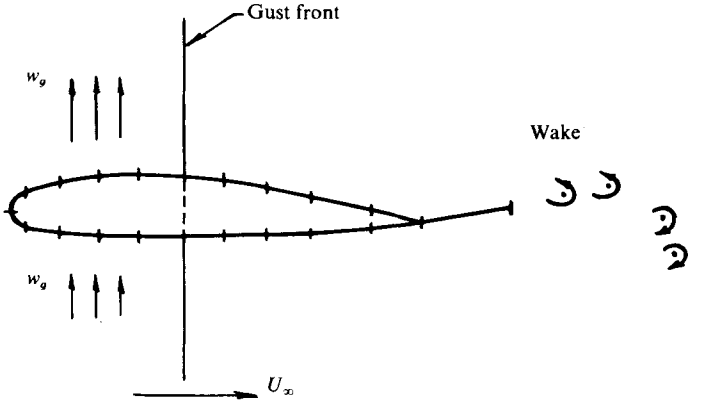

FIGURE 12. Model for undeformed gust front at time t_k.

numerical method has been applied to both cases, first assuming that the gust front does not deform, then allowing for gust deformation.

The problem for an undeformed gust boundary has been solved using directly the method outlined in § 2, where, as shown in figure 12, the gust velocity w_g modifies the tangency boundary conditions on those aerofoil elements which are behind the advancing gust front and in the gust field.

To allow the gust to deform the gust front is represented by a vortex sheet (figure 13). Between two chord lengths above and below the aerofoil this vortex sheet is divided into a number of straight-line elements of uniform vorticity, as shown in figure 13. The gust front is divided into elements of vorticity rather than point vortices for compatibility with the aerofoil singularity distributions. The two outer parts of the gust front extending to infinity above and below the aerofoil are assumed to remain undeformed and are therefore convected with the free-stream velocity. The straight-line elements representing the central part of the gust front are convected according to the local resultant velocities acting on them. The resultant velocities are calculated at the midpoints of each element and the resultant velocities at the ends of the elements are then obtained by interpolation. Thus the positions of these gust elements

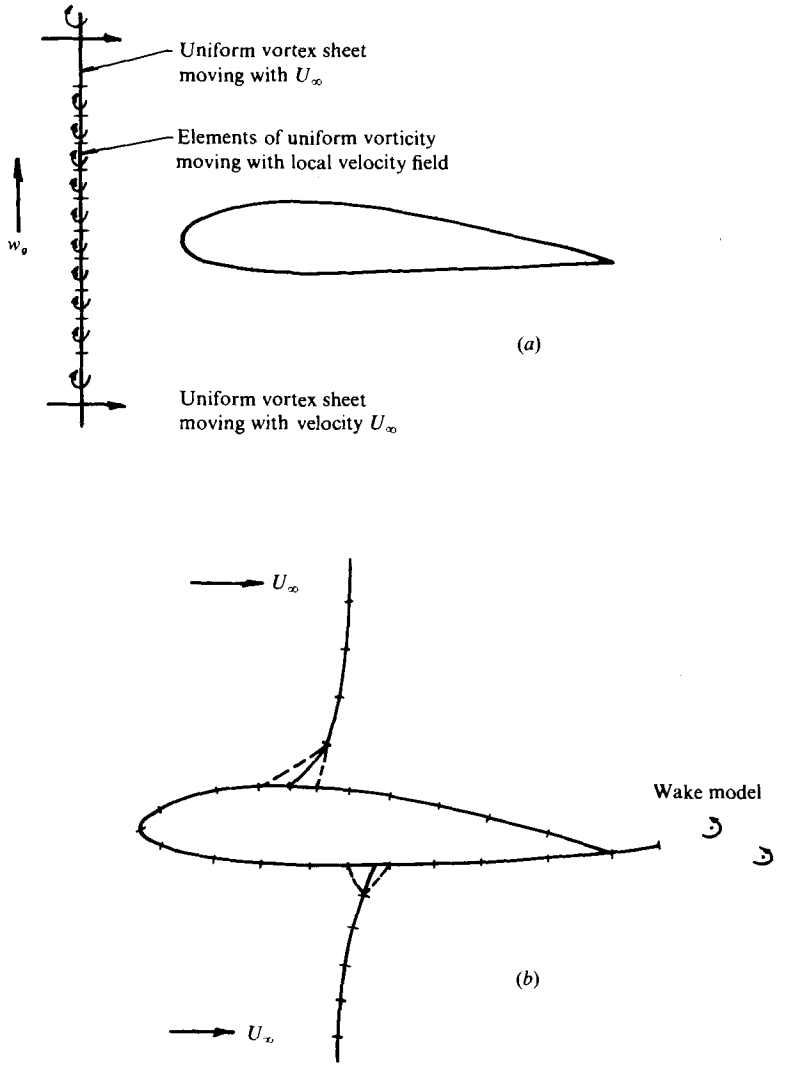

FIGURE 13. Model for the deformed gust front. (*a*) Gust front ahead of aerofoil. (*b*) Gust front passing over aerofoil.

at time t_k can be determined from their positions and velocity field at time t_{k-1}; the strength of the uniform vorticity on each element alters with a change in element length, but the total circulation around each element remains constant.

The calculation is performed in three stages. The first stage corresponds to the time before the gust front meets the leading edge of the aerofoil. The second stage corresponds to the time during which the gust front passes over the aerofoil. The third stage corresponds to the time when the gust front is beyond the aerofoil and passing through the wake. At each time step of the calculation the length, orientation and hence the vorticity strength of each element of the gust front are determined along with the singularity distributions on the aerofoil surface and the strength and position of the wake trailing-vortex system.

The first stage of the calculation is relatively simple, however some difficulties

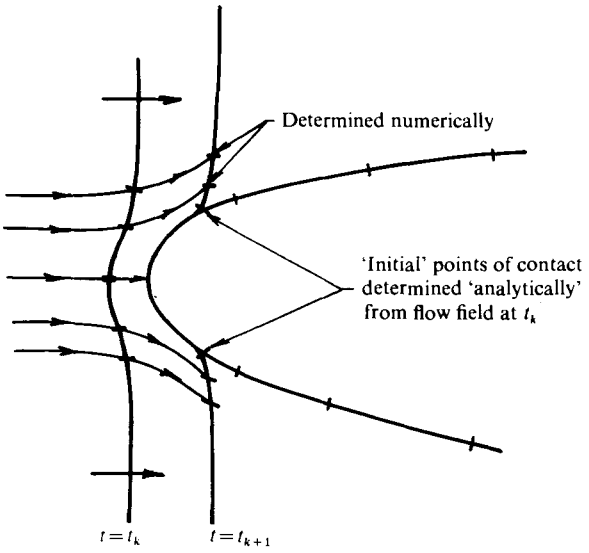

FIGURE 14. Attachment of the gust front to the aerofoil.

appear during the second stage. For example, at the instant just after the gust first 'hits' the aerofoil it is necessary to estimate the two 'initial' points of contact of the gust front with the aerofoil surface as the gust front divides into its upper and lower branches. These two 'initial' points of contact are determined approximately by assuming that the flow around the leading edge in the neighbourhood of the stagnation point when the gust front is just ahead of it is that past a circular cylinder of radius equal to the leading-edge radius (figure 14). Using this velocity field an estimate is made of the distance travelled by the gust elements in the neighbourhood of the leading edge from just upstream of the stagnation point to just behind it as the aerofoil enters the gust.

Another effect during this second stage concerns the motion of the points of contact of the gust front over the upper and lower aerofoil surfaces at successive time intervals since the points of contact should coincide with the ends of the elements on the aerofoil surface for numerical convenience. To meet this objective, as shown in figure 13(*b*), the element of the gust front adjacent to the aerofoil surface is replaced by two gust elements connecting the part of the gust front away from the aerofoil surface to the two edges of the nearest aerofoil surface element. The circulation around the gust 'element' in contact with the aerofoil surface is divided between the two arms in proportion to the distance of the contact point from the element's ends.

Since the velocities of the points of contact of the gust front on the upper and lower surfaces are different, the gust front leaves the two surfaces of the aerofoil at the trailing edge at different times. The third stage of the calculation, when the gust front traverses the wake is again straightforward, even though it involves the calculation of the wake pattern due to the mutual interference of the gust front and the wake vortex sheet.

Throughout the calculation the method gives the pressure distribution at each time step, from which the overall force and moment characteristics can be calculated.

The same aerofoil (i.e. an 8·4 % thick symmetrical Von Mises aerofoil) is considered

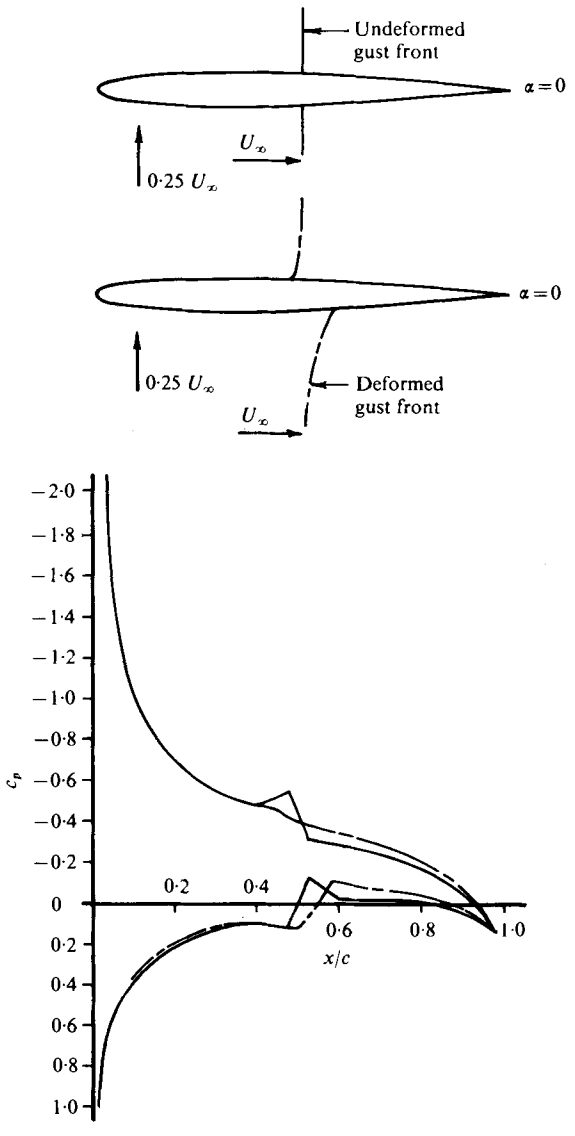

FIGURE 15. Entry of 8·4 % thick symmetrical Von Mises aerofoil into a sharp-edged gust. ——, undeformed gust front; — — —, deformed gust front.

for this calculation of an aerofoil passing through a sharp-edged gust. The vertical velocity of gust is taken to be $0{\cdot}25\ U_\infty$.

Figure 15 shows the pressure distributions as the gust passes over the aerofoil for both deformed and undeformed gust fronts when the aerofoil is initially at zero incidence. In the case of an undeformed gust boundary there is a sharp peak in the pressure distribution on both surfaces at the position of the gust front. This pressure peak diffuses out on the upper surface but not on the lower surface when the gust front is allowed to deform, owing presumably to the different curvatures of the gust front above and below the aerofoil. The pressure distributions over the forward part of the aerofoil which has entered the gust field are almost identical whether or not

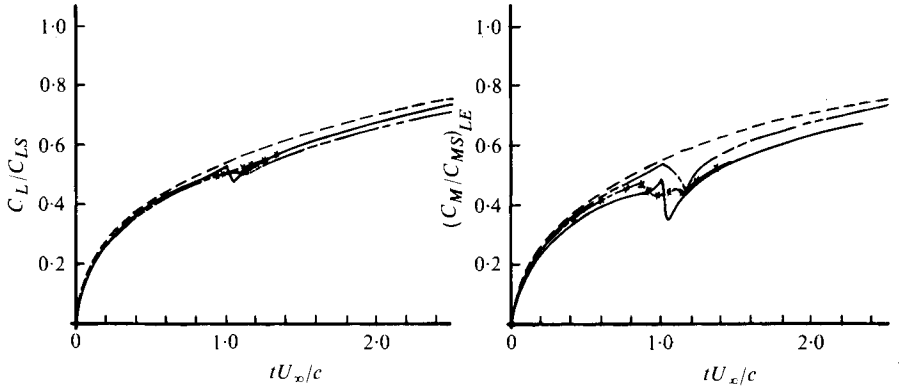

FIGURE 16. 8·4 % thick symmetrical Von Mises aerofoil entering a sharp-edged gust. ---, linearized theory; ——, undeformed gust, $\alpha = 0$; —×—, deformed gust, $\alpha = 0$; – – – –, deformed gust, $\alpha = 5°$.

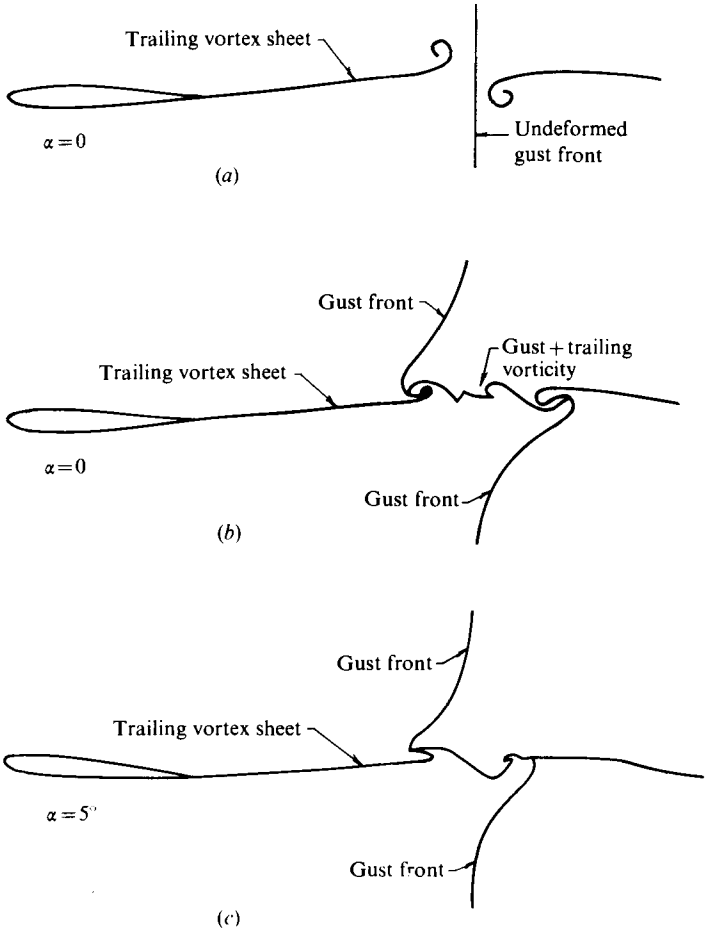

FIGURE 17. Wake patterns associated with a sharp-edged gust.

gust deformation is taken into account. However gust-front deformation changes the pressure distributions over the aft part of the aerofoil which has not yet entered the gust field. In spite of these differences, as indicated in figure 16, the overall lift and moments are not substantially different except when the gust is passing the trailing edge; the results for the undeformed gusts show sudden changes in the lift and moment while gust deformation appears to smooth out these abrupt variations. Calculations have also been carried out with the aerofoil at a mean incidence; the effect of mean incidence is indicated most clearly in the moment curve in figure 16, where there is a lag effect as the gust front passes the trailing-edge region since incidence modifies the progression of the gust front over the upper and lower aerofoil surfaces.

As the gust progresses down the wake, as shown in figure 17, there is a considerable difference in the wake patterns for deformed and undeformed gust fronts. This difference is a measure of how the wake is affected by the mutual interaction of the wake vortex system and the vortex sheet representing the gust front. It is seen in figure 17(*c*) that incidence does not introduce any significant change in the wake characteristics. One possible practical implication of these wake patterns is to raise the question of the accuracy of calculations of the forces on a tailplane in the downwash field of a main wing when the aircraft enters a sharp-edged gust.

6. Concluding remarks

The numerical method outlined in this paper leads to the calculation of the inviscid flow field about an aerofoil undergoing an arbitrary time-dependent motion if it is assumed that the flow remains attached and that it separates at the trailing edge of the aerofoil. Although results have been presented for a sudden change in incidence, a high frequency oscillation and entry into a sharp-edged gust, the method is completely general.

REFERENCES

Basu, B. C. & Hancock, G. J. 1978 Two dimensional aerofoils and control surfaces in simple harmonic motion in incompressible inviscid flow. *Aero. Res. Coun. Current Paper* no. 1392.

Giesing, J. P. 1968 Non-linear two-dimensional unsteady potential flow with lift. *J. Aircraft* **5** (2), 135.

Giesing, J. P. 1969 Vorticity and Kutta condition for unsteady multi-energy flows. *Trans. A.S.M.E., J. Appl. Mech.* **91**, 608.

Glauert, H. 1947 *The elements of Aerofoil and Aircrew Theory*, 2nd edn. Cambridge University Press.

Hancock, G. J. & Padfield, G. 1972 Numerical solution for steady two-dimensional aerofoils in incompressible flow. *Queen Mary Coll. Rep.* EP-1003.

Hess, J. L. & Smith, A. M. O. 1967 Calculation of potential flow about arbitrary bodies. *Prog. Aero. Sci.* **8**, 1.

Maskell, E. C. 1972 On the Kutta–Joukowski condition in two-dimensional unsteady flow. Unpublished note, Roy. Aircraft Establishment, Farnborough.

Vooren, A. I. van der & Vel, H. van der 1964 Unsteady profile theory in incompressible flow. *Arch. Mech. Stosowanej* **3**.